relationship between molecular structure and the mesomorphic phase of thermotropic liquid crystals. The phase behavior in our rod–coil system can be explained by the fact that the main factor governing the geometry of the supramolecular architecture in the liquid-crystalline phase is the anisotropic aggregation of rod segments and the consequent space-filling requirements as well as entropic limitations due to the flexibility of the coil.[10–13] The lamellar structure observed in the crystalline phase for **3** or in the liquid -crystalline phase for **1** is still the most efficient packing of melt chains, which is similar to that of smectogens with low molar mass. With increasing temperature (in the case of **3**) or increasing volume fraction of coil segments, however, space crowding of the coil segments would be larger. Lamellar ordering of rods would confine junctions between rods and coils to a flat interface with a relatively high density of grafting sites, which forces a strong stretching of the coils away from the interface, and the system becomes energetically unfavorable. Consequently, the lamellar structure of the rod–coil molecule will break apart into interwoven networks of branched cylinders to lead to a bicontinuous cubic phase and then discrete cylinders; this gives rise to a hexagonal columnar phase in which coil stretching is reduced.

Although this explanation is qualitatively consistent with theoretical predictions for the phase behavior of rod–coil diblock molecules, that of our system is in contrast to the predicted specific supramolecular structures such as the various "hockey-puck" phases.[11] In this respect, our system provides access to a large variety of experimental and theoretical investigations to understand fully the complete range of supramolecular structures formed by rod–coil diblock molecules. This is essentially an unexplored area of research.

In summary, the rod–coil molecules which can be considered as either small diblock copolymers or large smectogens were observed to organize into bicontinuous cubic and hexagonal columnar mesophases as a function of volume fraction of the coil segments or temperature. This behavior differs significantly from that predicted for this type of molecule.[10–13]

Received: September 2, 1997 [Z 10881 IE]
German version: *Angew. Chem.* **1998**, *110*, 661–663

Keywords: columnar phases · cubic phases · liquid crystals · mesophases · supramolecular chemistry

[1] "Liquid Crystals": H. Stegemeyer, *Top. Phys. Chem.* **1994**, *3*.
[2] M. A. Hillmyer, F. S. Bates, K. Almdal, K. Mortensen, A. J. Ryan, J. P. Fairclough, *Science* **1996**, *271*, 976–978; F. S. Bates, *ibid.* **1991**, *251*, 898–901; S. Foster, A. K. Khandpur, J. Zhao, F. S. Bates, I. W. Hamley, A. J. Ryan, W. Bras, *Macromolecules* **1994**, *27*, 6922–6935.
[3] J. T. Chen, E. L. Thomas, C. K. Ober, G. Mao, *Science* **1996**, *273*, 343–346; J. T. Chen, E. L. Thomas, C. K. Ober, S. S. Hwang, *Macromolecules* **1995**, *28*, 1688–1697; L. H. Ladzilowski, B. O. Carraher, S. I. Stupp, *ibid.* **1997**, *30*, 2110–2119; L. H. Ladzilowski, S. I. Stupp, *ibid.* **1994**, *27*, 7747–7753; S. I. Stupp, V. LeBonheur, K. Walker, L. S. Li, K. E. Huggins, M. Keser, A. Amstutz, *Science* **1997**, *276*, 384–389. We thank a referee for bringing our attention to this work.
[4] M. Lee, N.-K. Oh, *J. Mater. Chem.* **1996**, *6*, 1079–1086.
[5] M. Lee, N.-K. Oh, H.-K. Lee, W.-C. Zin, *Macromolecules* **1996**, *29*, 5567–5573; M. Lee, N.-K. Oh, *Mol. Cryst. Liq. Cryst.* **1996**, *280*, 283–288.
[6] M. Lee, N.-K. Oh, W.-C. Zin, *Chem. Commun.* **1996**, 1787–1788.
[7] D. Demus, L. Richter, *Texture of Liquid Crystals*, Verlag Chemie, Weinheim, **1978**; G. W. Gray, J. W. Goodby, *Smectic Liquid Crystals, Texture and Structures*, Leonard Hill, Glasgow, **1984**.
[8] C. Destrade, P. Foucher, H. Gasparoux, N. H. Tinh, A. M. Levelut, J. Malthete, *Mol. Cryst. Liq. Cryst.* **1984**, *106*, 121–146; C. Destrade, N. H. Tinh, H. Gasparoux, J. Malthete, A. M. Levelut, *ibid.* **1981**, *71*, 111–117.
[9] J. M. Seddon, *Biochemistry* **1990**, *29*, 7997–8002; V. Luzzati, P. A. Spegt, *Nature* **1967**, *215*, 701–704.
[10] A. N. Semenov, *Mol. Cryst. Liq. Cryst.* **1991**, *209*, 191–199; A. N. Semenov, S. V. Vasilenco, *Sov. Phys. JETP Engl. Transl.* **1986**, *63*, 70–79.
[11] D. R. M. Williams, G. H. Fredrickson, *Macromolecules* **1992**, *25*, 3561–3568.
[12] A. Halperin, *Macromolecules* **1990**, *23*, 2724–2731.
[13] E. Raphael, P. G. de Gennes, *Makromol. Chem. Macromol. Symp.* **1992**, *62*, 1–17.

Superconductivity and Chemical Bonding in Mercury

Shuiquan Deng, Arndt Simon,* and Jürgen Köhler

Dedicated to Professor Hartmut Bärnighausen on the occasion of his 65th birthday

Recently a hypothesis on the chemical origin of superconductivity was proposed which is based on a tendency for pairwise localization of conduction electrons.[1] In crystalline phases, in which chemical bonding is adequately described by the electronic band structure, a prerequisite for superconductivity seems to be the simultaneous occurrence of bands with large dispersion, "steep bands", and those with "flat bands" at the Fermi level E_F. The flat bands provide a vanishing Fermi velocity for some conduction electrons in the normal conducting state. This view is formally similar to a physical model based on the interplay of itinerant electrons in a wide band with local pairs of electrons in a narrow band.[2] However, in extracting the flat band/wide band features from calculated band structures we address the specific chemical bonding in actual superconductors.

Following arguments introduced by Krebs,[3] who suggested that the necessary condition for superconductivity is a crystal orbital that is nodeless in certain directions, Johnson and Messmer used SCF-Xα-SW cluster calculations to obtain remarkably accurate results for the superconducting characteristics of a number of elements and compounds.[4] However, this real space approach is based on clusters rather than infinite solids; in terms of a band structure, Γ point configurations are considered.

[*] Prof. Dr. A. Simon, Dr. S. Deng, Dr. J. Köhler
Max-Planck-Institut für Festkörperforschung
Heisenbergstrasse 1, D-70569 Stuttgart (Germany)
Fax: (+49) 711-689-1091
E-mail: remon@simpow.mpi-stuttgart.mpg.de

  1433-7851/98/3705-0640 $ 17.50+.50/0

Superconductivity has been discovered with mercury (T_c = 4.2 K).[5] Here we report on our studies of the electronic properties of the metal at the normal conducting state based on calculations of the Fermi surface, the total density of states (DOS), and the orbital analysis of the projected band structure. We are particularly interested in the occurrence of flat bands at the Fermi level E_F, and the character of chemical bonding for the states that belong to these bands. The term flat band refers to a section of a band, which falls into a narrow energy window centered by E_F, where the group velocities of the electrons approach zero. The width of the energy window should correspond to the Debye frequency; however, to account for inaccuracies of the band structure calculation, the window was fixed at a forty times larger value. We used the LMTO method[6] to calculate the energy dispersion $E(\boldsymbol{k})$ in the irreducible Brillouin zone (BZ).[7] After $E(\boldsymbol{k})$ was obtained, the scalar velocity field[12] in the whole BZ was calculated, and the maximum velocity as well as the positions and shapes of the flat bands were determined, the latter by using our own program.[13] The regions of the flat band are quite small. In order to analyze their bonding properties it is sufficient to choose one $\boldsymbol{k}$ point. Crystal orbital overlap population (COOP) curves[14] at some individual $\boldsymbol{k}$ point—not averaged over the entire BZ—were used as a bonding indicator for the flat band. To achieve this, we used the semiempirical extended Hückel (EH) method[15, 16] to carry out the bonding analyses.[17] The obtained bands below E_F were in good agreement with the LMTO bands.

The band structure of Hg serves as a particularly easy-to-analyze example to illustrate the flat band/steep band scenario. As Figure 1 shows, the total DOS at E_F has no local maximum and is very low ($N(E_F) = 0.29$ states/(eV · cell)). The bands have 6p and 6s character. The narrow 5d bands lie 5.6 to 8.7 eV below E_F. Hence, the electrons in the d bands do not contribute to the metallic and superconducting properties of Hg. Figure 1 also shows the energy dispersion $E(\boldsymbol{k})$ for seven bands up to E_F along three symmetry lines in the BZ.

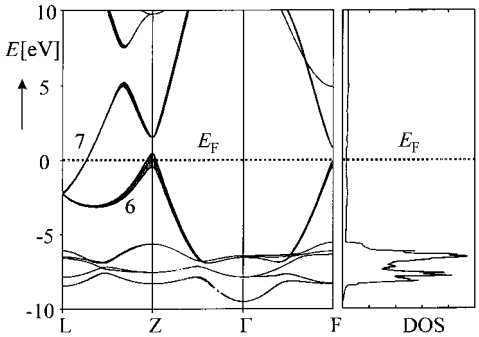

Figure 1. Band structure calculated for special symmetry directions and the total DOS of Hg. The fatness of the bands illustrates the contribution of the p_z orbital.

The highest occupied band (band 7) crosses the Fermi level, while the maxima of the next lowest band (band 6) approaches E_F at the Z and F points. It is worth mentioning that band 6 crosses E_F in other parts of the BZ. The flat bands at F and Z exhibit pure p character as p (ungerade) does not mix with s (gerade) at the special points. The "fat band" representation indicates the exclusive p_z orbital character of the flat band in Z (see below). In agreement with earlier results obtained both by relativistic APW calculations[18] and by de Haas–van-Alphen measurements,[19] our calculated Fermi surface (Figure 2) is composed of six electronic lenses (band 7) centered at the large hexagonal faces and a multiply connected surface of holes (band 6). The Fermi velocity on each lens decreases from the face center to the edge of the lens, while that on the multiply connected Fermi surface is low when it rides on the edge of the large hexagonal face of the BZ, and high when it rides on the edge of the rectangular face.

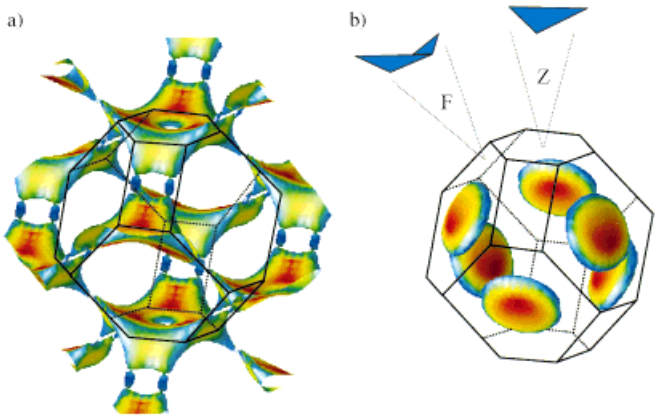

Figure 2. Fermi surface of Hg for band 6 (a) and band 7 (b) (Brillouin zone outlined). The increasing velocity of the electrons is represented by the change from blue to red. The isovelocity surface for band 6 around the F and Z points at a value of 0.03 (atomic units) is additionally shown in b). The two features are magnified by a factor of 100; they lie within the range of $E_F \pm 0.28$ eV.

Band 7, the steep band, crosses the Fermi level with various velocities throughout the BZ; the largest value is 1.29 (in atomic units). The highest value for the velocity of electrons within the energy window of $E_F \pm 0.28$ eV is 1.88 for band 7 and 1.83 for band 6. The maxima of band 6 at Z and F, which fall into the same energy window, meet the flat band, where the electron velocities become zero. In the energy window $E_F \pm 0.28$ eV this special condition only holds for these two $\boldsymbol{k}$ points in the whole BZ. Hence, the great majority of the conduction electrons exhibits high velocities. In this energy window the isovelocity surface at a value of 0.03 is plotted for band 6 in Figure 2, illustrating the shapes and locations of the flat band characteristics and giving evidence for their very limited extensions.

The self-consistently calculated and the fitted semiempirical band structure are in good agreement for all bands up to E_F, which provides added support for the accuracy of the analysis of the bonding properties of the flat bands on the basis of the semiempirical results. The interaction between nearest neighbors (2.986 Å) averaged over the whole BZ is of weakly bonding character for the band states around E_F. This particularly holds for the flat band states in band 6, as can be shown more explicitly with COOP curves calculated specifically for the Z and F points.

  1433-7851/98/3705-0641 $ 17.50+.50/0

The crystal orbital of Hg at the Z point is purely p_z character (see Figure 1), as revealed by LMTO and EH calculations, while at the F point the orbital is a hybrid of Hg p_z, p_y, and p_x orbitals (with dominating p_z contribution). The crystal orbitals in band 6 are plotted for the Z and F point, respectively, in Figure 3. In both cases the imaginary part of the crystal orbital is very small and thus neglected. The crystal orbital at Z has the D_{3d} symmetry of the Z point in the BZ, while that at F has C_{2h} symmetry.

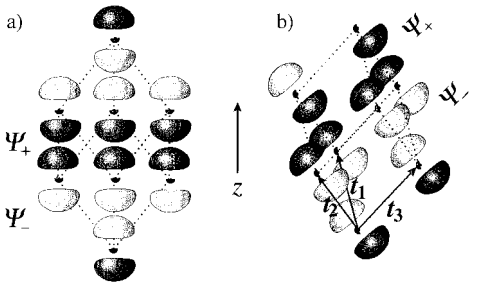

Figure 3. The crystal orbitals at Z (a) and F (b) in band 6. In a) the state is composed of pure p_z, while in b) the orbital at the origin of the primitive lattice is a hybrid of $-0.2642p_x$, $-0.4577p_y$, and $-0.5633p_z$. In both cases, the Ψ_+ and Ψ_- indicate two nodeless bonding systems, which are composed of the positive and the negative lobes of the orbitals, respectively.

At Z the orbital interactions along all three primitive lattice vectors (2.986 Å) are of $\sigma(p_z-p_z)$ type, while that along the short face diagonal direction (3.457 Å) is of $\pi(p_z-p_z)$ type. However, as the lobes of the p_z orbital do not point directly in the directions of the lattice vectors, the σ bonding is quite weak. At the F point, the orbital interactions along $\boldsymbol{t}_1$ and $\boldsymbol{t}_2$ are of σ(p – p) type, while those along the $\boldsymbol{t}_3$ direction are of π(p – p) type. In the $\boldsymbol{t}_1\boldsymbol{t}_2$ plane the orbital interactions along the $\boldsymbol{t}_1-\boldsymbol{t}_2$ direction are also of π(p – p) type, while those in the $\boldsymbol{t}_1\boldsymbol{t}_3$ and $\boldsymbol{t}_2\boldsymbol{t}_3$ planes are of σ(p – p) type. As shown in Figure 3a, for the Z point, $\pi(p_z\text{-}p_z)$ bonding occurs in planes perpendicular to the threefold axis and results in layers without nodes. Nodes occur between adjacent layers. According to Figure 3b, at the F point the nodeless bonding systems occur in layers that are oblique to the threefold axis, and these layers are again separated by nodal planes. The topologies of the crystal orbitals of the flat bands perfectly agree with those thought to be essential for superconductivity.[3, 4]

Our results suggest a rather visual scenario for the occurrence of superconductivity in mercury (and other conventional superconductors). According to the band structure the conduction electrons in mercury have large Fermi velocities except for a few that are at rest. The latter need to become singlet electron pairs in order to undergo condensation into the superconducting state.[20] Pairing can be achieved by coupling of the flat band states to dynamical lattice distortions, phonons, which modulate the bonding character of the band states in the maxima. A sufficient lowering of these states provides the spin pairing energy. Phonons periodically change the position of the flat band relative to E_F, and when the top of the flat band lies above E_F the electron pairs are scattered into states of steep bands near E_F. Vice versa, the electrons scatter into the so-created empty flat band states to become paired. At T_c the paired state becomes stable through condensation, and as the flat band states are periodically depleted they are continuously filled from the large reservoir of electrons in steep bands, thus creating more and more bosons.

Provided our hypothesis is correct, then two aspects are worth mentioning. First, in the band structure of Hg flat bands only lie at E_F when relativistic effects are considered in the calculations, otherwise the flat bands are located approximately 1 eV below E_F. Hence, mercury is a relativistic superconductor. Second, the flat bands have such tiny extensions that the identification of this feature, if responsible for superconductivity, rather resembles the search for a needle in a haystack.[21]

Received: September 3, 1997 [Z10888IE]
German version: *Angew. Chem.* **1998**, *110*, 664 – 666

Keywords: ab initio calculations · bond theory · extended Hückel calculations · mercury · superconductors

[1] A. Simon, *Angew. Chem.* **1997**, *109*, 1873; *Angew. Chem. Int. Ed. Engl.* **1997**, *36*, 1788.
[2] V. B. Geshkenbein, L. B. Ioffe, A. I. Larkin, *Phys. Rev. B* **1997**, *55*, 3173; J. Ranninger, J. M. Robin, *Physica C* **1995**, *253*, 279; R. Micnas, J. Ranninger, S. Robaszkiewicz, *Rev. Modern Phys.* 1990, 62, 113; A. S. Alexandrov, J. Ranninger, *Phys. Rev.* B **1981**, *23*, 1796; *ibid.* **1981**, *24*, 1164; J. Ranninger in *Polarons and Bipolarons in High-T_C Superconductors and Related Materials*, (Eds.: E. K. H. Salje, A. S. Alexandrov, W. Y. Liang), Cambridge University Press, Cambridge, **1995**, p. 67.
[3] H. Krebs, *Prog. Solid State Chem.* **1975**, *9*, 269.
[4] K. H. Johnson, R. P. Messmer, *Synthetic Metals* **1983**, *5*, 151.
[5] H. Kamerlingh-Onnes, *Akad. van Wetenschapen (Amsterdam)* **1911**, *14*, 113.
[6] Self-consistent first-principles linear muffin-tin orbital method: O. K. Andersen, O. Jepson, M. Sob in *Electronic Band Structure and its Applications* (Ed.: M. Yussouff), Springer, Berlin, **1986,** p. 1 – 57.
[7] The "combined correction"[8] to the atomic sphere approximation was used to get more accurate one-electron Hamiltonian and overlap matrices. The exchange-correlation potential of the density functional theory was obtained in the local density approximation (LDA) applied by Barth and Hedin.[9] The scalar-relativistic effect was considered through this calculation by solving the Dirac rather than the Schrödinger equation. All $\boldsymbol{k}$ space integrations were performed with the tetrahedron method[10] by using 4237 irreducible $\boldsymbol{k}$ points, and basis sets of 6s, 6p, 5d, and 5f orbitals; the 5f orbitals were down-folded.[11] These orbitals can carry charges, but make no contributions to the dimensions of Hamiltonian and overlap matrices, which saves calculation time and avoids possible distortions for the phase shifts of the high partial waves, or even the ghost band. To avoid too large atomic sphere overlap (1.6842 Å), we inserted an interstitial sphere with a radius of 0.8924 Å into the structure at (0,0,0.8832). Thus the actual basis set for the Hg calculations also includes 1s and 2p LMTOs of the interstitial, with 2p down-folded at the same level as that of the above-mentioned f orbitals.
[8] O. K. Andersen, *Phys. Rev.* B **1975**, *12*, 3060.
[9] U. von Barth, L. Hedin, *J. Phys.* C **1971**, *4*, 2064.
[10] P. Blöchl, O. Jepsen, O. K. Andersen, *Phys. Rev.* B **1994**, *49*, 16223.
[11] W. R. L. Lambrecht, O. K. Andersen, *Phys. Rev.* B **1986**, *34*, 2439.
[12] The group velocity of an electron is defined as $\boldsymbol{v}(\boldsymbol{k})=(1/\hbar)\nabla_k E(\boldsymbol{k})$, however, we use the term "velocity" for the scalar $v(\boldsymbol{k})=\sqrt{v(k)\cdot v(k)}$.
[13] S. Deng, Max-Planck-Institut für Festkörperforschung, Stuttgart **1997**.
[14] T. Hughbanks, R. Hoffmann, *J. Am. Chem. Soc.* **1983**, *105*, 3528.
[15] G. A. Landrum, YAeHMOP: Another EHMO package, Cornell University, Ithaca, NY (USA), **1997**.

  1433-7851/98/3705-0642 $ 17.50+.50/0

[16] The structural data used in this calculation are $a = 2.986$ Å, $\alpha = 70.743$, space group $R\bar{3}m$. All calculations are based on the primitive unit cell rather than the conventional one.The symbols of special $\boldsymbol{k}$ points in the BZ and the Cartesian system have been taken from Bradely and Cracknell.[17] EH parameters: H_{ii} [eV] (coefficients ζ_1) for Hg: 6s −13.68 (2.649), 6p −8.47 (2.631); 5d −17.50 (6.436); double ς functions were used: 5d C_1 0.6438, ς_2 3.032, and C_2 0.5215.
[17] C. J. Bradely, A. P. Cracknell, *The Mathematical Theory of Symmetry in Solids*, Clarendon, Oxford, **1972**.
[18] S. C. Keeton, T. L. Loucks, *Phys. Rev.* **1966**, *146*, 429; *ibid.* **1966**, *152*, 548; *ibid.* **1968**, *168*, 672.
[19] G. B. Brandt, J. A. Rayne, *Phys. Rev.* **1966**, *148*, 644.
[20] F. London, *Phys. Rev.* **1938**, *54*, 947.
[21] Calculations on the other polymorphs of mercury would serve as test cases for our criteria on the occurrence of superconductivity, however, the lack of knowledge concerning the structures prevents such calculations.

Stilbenoid Dendrimers**

Herbert Meier* and Matthias Lehmann

Stilbenoid compounds show interesting photophysical and photochemical properties and are therefore appropriate for various applications in materials science.[1] Besides use in well-established areas such as optical brighteners, new applications are increasingly becoming apparent, including light-emitting diodes (LED), nonlinear optics (NLO), and optical imaging, storage, and switching techniques.

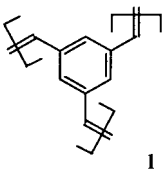

1

Through the incorporation of stilbenoid chromophores into dendrimers,[2] the design of which is also of considerable interest, we envisioned the new structural concept **1**. The convergent syntheses, coupled for individual generations, are depicted in Schemes 1 and 2. The required *E*-configured double bonds were formed by the Wittig–Horner reaction. The readily available tris(phosphonate) **3**[3] was used as a basic unit to form the core. Aldehyde **8**[4] and the bis(phosphonic acid) derivative **7**[5] with a protected aldehyde functionality served as building blocks for generating the dendrons; aldehydes **9**[6] and **10**[7] were obtained via **7** (Scheme 1). This procedure permitted the preparation of three generations of dendrimers (**1a**–**c**) from **3** and **8**, **9**, and **10** (Scheme 2). Tris(dodecyloxy)phenyl groups were attached to the periphery in order to enhance solubility and, as discussed below, to induce liquid crystalline (LC) behavior. The *trans* selectivity of the Wittig–Horner reaction is sufficiently high in this series of stilbenoid compounds to generate all-*trans* isomers **1a**–**c** within the limits of NMR detection. ^{1}H and ^{13}C NMR spectroscopy confirms the threefold symmetry of dendrimers **1a**–**c**. The observed chemical shifts are all very similar within this series of compounds (Table 1).

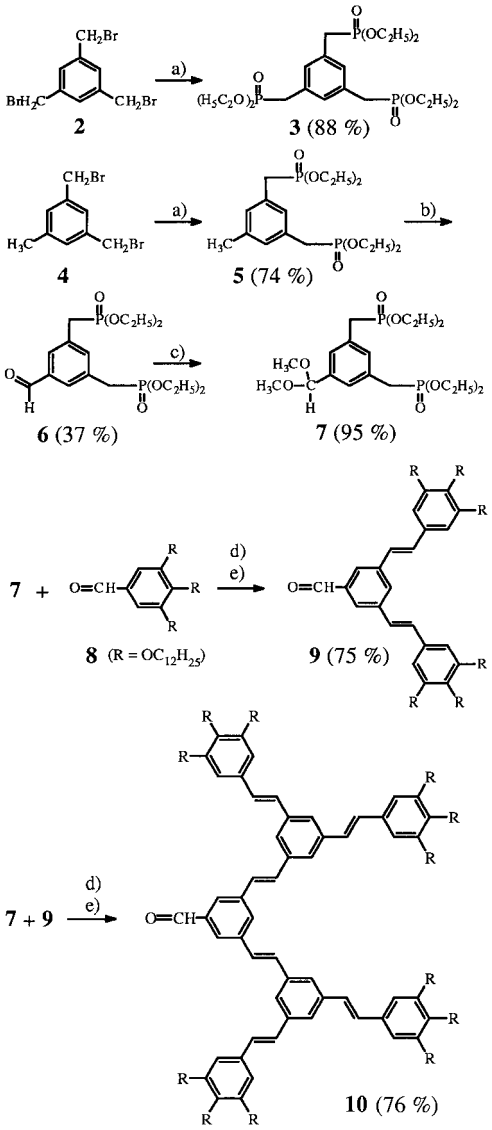

Scheme 1. Synthesis of the dendrimer precursors. a) $P(OC_2H_5)_3$, 160 °C; b) NBS (CCl_4), Fe (H_2O), 100 °C; c) CH_3OH, $HC(OCH_3)_3$, Dowex 50W-X8; d) $KOC(CH_3)_3$ (THF); e) HCl ($CHCl_3$).

The MALDI-TOF technique proved to be excellent for determining the molecular masses of **1a**–**c**. The discrepancy between the measured and calculated *m/z* values amounts to no more than one mass unit. For example, for **1c** with the molecular formula $C_{606}H_{996}O_{36}$ we obtained the value 8859.6, whereas the calculated mean for the peak of this molecular ion M^+ is 8858.6. The yields presented in Scheme 2 refer to dendritically pure compounds whose formation is assured by the convergent synthesis. A small amount of the "two-branched" compound, formed when only two molecules of **10** reacted with **3**, could only be detected in the crude product of **1c** with the MALDI-TOF method.

The aggregation of the stilbenoid dendrimers is especially interesting. Neat **1a** and **1b** generate two liquid crystalline phases each (D_{hd}: discotic hexagonal disordered phase; D_{rd}: discotic rectangular disordered phase; D_{ob}: discotic oblique

[*] Prof. Dr. H. Meier, Dipl.-Chem. M. Lehmann
Institut für Organische Chemie der Universität
J.-J. Becherweg 18-22, D-55099 Mainz (Germany)
Fax: (+49) 6131 395-396
E-mail: hmeier@mzdmza.zdv.uni-mainz.de

[**] This work was supported by the Deutsche Forschungsgemeinschaft and the Fonds der Chemischen Industrie.